Vol. 20, No. 1 (2021) 67-75
Revista Mexicana de Ingeniería Química
Materiales

Cobalt and copper nanoparticles on partially reduced graphene oxide interlayer spacing carbon nanotubes or carbon black as catalysts for oxygen reduction reaction

Nanopartículas de cobalto y cobre sobre óxido de grafeno parcialmente reducido con espaciadores de nanotubos de carbono o carbón vulcano como catalizadores para la reacción de reducción de oxígeno

Y.Y. Rivera-Lugo[1], C. Silva-Carrillo[1], B. Trujillo-Navarrete[1], E.A. Reynoso-Soto[1], T. Romero-Castañón[2], S.W. Lin-Ho[1], J.C. Calva-Yañez[3], F. Paraguay-Delgado[4], R.M. Félix-Navarro[1]*

[1]*Centro de Graduados e Investigación en Química, Tecnológico Nacional de México/Instituto Tecnológico de Tijuana, Blvd. Alberto Limón Padilla, S/N, Otay Tecnológico, Tijuana, B.C., 22500, México.*
[2]*Instituto Nacional de Electricidad y Energías Limpias, Reforma 113, Palmira, Morelos. C.P. 62490, México.*
[3]*CONACyT-Tecnológico Nacional de México/IT Tijuana, Centro de Graduados e Investigación en Química, Blvd. Alberto Limón Padilla, S/N, Otay Tecnológico, Tijuana, B.C., 22500, México.*
[4]*Centro de Investigación en Materiales Avanzados SC, Miguel de Cervantes 120, C.P. 31136, Chihuahua, Mexico*

Received: November 1, 2019; Accepted: May 22, 2020

Abstract

In this paper, we reported the synthesis of Co and Cu nanoparticles (NPs) supported on partially reduced graphene oxide (M/rGO), with the incorporation of spacers as multi-walled carbon nanotubes (MWCNT) and carbon black (CB) among graphene interlayers to generate carbon nanocomposites. The oxygen reduction reaction (ORR) polarization curves show that the use of MWCNT as spacer improves the current density up to 6.9 times for Co NPs and up to 3.5 times for Cu NPs materials. Also, the charge transfer resistance decreases using CB: 950 times for Co NPs and 68 for Cu NPs materials. All carbon-nanocomposites present upgraded stability comparing to the commercial platinum catalyst (Pt/C).
Keywords: ORR, spacers, graphene, nanocomposites, Pt-free catalysts, fuel cells, alkaline, power generation.

Resumen

En este trabajo, reportamos la síntesis de nanopartículas (NPs) de Co y Cu soportadas sobre óxido de grafeno parcialmente reducido (M/rGO), con la incorporación de espaciadores como nanotubos de carbono de pared múltiple (MWCNT) y carbón vulcano (CB) entre las láminas de grafeno para generar nanocompositos de carbono. Las curvas de polarización de la reacción de reducción de oxígeno (RRO) muestran que el uso de MWCNT como espaciadores mejora la densidad de corriente hasta 6.9 veces para los materiales de Co NPs y hasta 3.5 veces para Cu NPs. Además, la resistencia a la transferencia de carga disminuye usando CB: 950 veces para los materiales Co NPs y 68 para Cu NPs. Todos los nanocompositos de carbono presentaron una mejor estabilidad comparada con el catalizador de platino comercial (Pt/C).
Palabras clave: RRO, espaciadores, grafeno, nanocompositos, catalizadores libres de Pt, celdas de combustible, alcalina, generación de energía.

1 Introduction

Fossil fuel energy consumption as a primary energy source is inviable, generating the air, soil, and water pollution (Ediger, 2019; Flores *et al*., 2008; Ortiz-Salinas *et al*., 2012). Nowadays, protecting and preserving our environment is a priority. One alternative is the energy generation using environment-friendly technologies. Where the fuel cell can play an essential role in the solution. This device converts the chemical potential energy into electrical energy by means a continuous supply of reagents, getting only water and heat as sub-products (Arshad *et al*., 2019). For the alkaline membrane fuel cells (AMFC), the involved reactions are the oxygen

* *Corresponding author. E-mail*: rmfelix@tectijuana.mx
https://doi.org/10.24275/rmiq/Mat961
ISSN:1665-2738, *issn-e*: 2395-8472

reduction (ORR, cathodic) and hydrogen oxidation (HOR, anodic) (Pan *et al*., 2018).

For instance, the cathodic reaction is dominated by the electron transfer and the bonding energy to oxygen, where Pt^0 is the cathodic catalyst that presents the best performance (Norskov *et al*., 2004). However, its high-cost and low abundance limit its application on a large scale (Valdez-Ojeda *et al*., 2014). There is an essential need to develop efficient methodologies to get Pt free catalysts, where the support selection is vital. The supported catalyst must be chemically stable in order to prevent corrosion as well as a good electrical conductor. The graphene is one most used carbonaceous supports (Akhina *et al*., 2019; Akhina *et al*., 2017). However, the large surface area provided by graphene can decrease, and this can be promoted by the high surface energy of the dangling bonds this need to restacking in a large number of sheets (Wu *et al*., 2020; Korkmaz and Kariper, 2020). One strategy to prevent the restacking is the use of spacers, e.g., carbon black (CB) and multiwalled carbon nanotubes (MWCNT) interlayer graphene sheets, which are known as carbon nanocomposites (Yurtcan and Daş, 2018; Yilmaz *et al*., 2019; Song *et al*., 2019; Mukherjee *et al*., 2019). These nanomaterials have an increase in the specific surface area and conductivity; enhanced electrochemical performance; and decrease the Pt use (Marinkas *et al*., 2013). For example, Park *et al*. (2011) reported a Pt catalyst supported on graphene-carbon black hybrids; they found that CB changes the array of graphene supports, resulting in more Pt nanoparticles (NPs) available as a catalyst. Also, Yang *et al*. (2019) established that the CB spacer use has a lower charge transfer resistance than CNT. Huang *et al*. (2012) and Li *et al*. (2018) informed that the use of carbon spacers improved the activity of the Pt catalyst and its stability.

Another strategy is the use of non-noble metals. In the literature, several reports have been confirmed that Pt can be substituted using non-noble metals in alkaline media (Vanýsek, 2009; Shahid *et al*., 2017). These works have attracted the attention of the researchers, who have proposed a range of non-noble metals to substitute Pt content in ORR (Garapati *et al*., 2019; Yan *et al*., 2018). However, few studies have investigated non-noble metals NPs in any systematic way in carbon nanocomposites. In this work, we reported an eco-friendly method to synthesize carbon nanocomposites of Co NPs or Cu NPs on partially reduced graphene oxide (rGO) using as spacers MWCNT and CB, testing them as a catalyst for ORR in alkaline media.

2 Experimental

All chemicals reagents received without further purification copper sulfate ($CuSO_4{\cdot}5H_2O$, 98%), ferrocene ($Fe(C_5H_5)_2$, 98%), Nafion® 117 solution (5%), sodium borohydride ($NaBH_4$, 99%), sodium nitrate ($NaNO_3$, ≥99%) and cobalt (II) chloride anhydrous ($CoCl_2$, 97%) were purchased from Aldrich. Ethanol (CH_3CH_2OH, 95%), acetone (CH_3COCH_3, 99.5%), sulfuric acid (H_2SO_4, 98%), nitric acid (HNO_3, 70%) and hydrogen peroxide (H_2O_2, 30%) were acquired from Faga Lab. Graphite, manganese (II) sulfate ($MnSO_4{\cdot}H_2O$, 100%), toluene ($C_6H_5CH_3$, 99.5%), potassium permanganate ($KMnO_4$, 98%), and carbon black were supplied from Fisher Chemical, Fermont, JT Baker®, Alfa-Aesar and Fuel Cell Store©, respectively. All aqueous solutions were prepared with Milli-Q® water (18 MΩ, Millipore). Also, we synthesized MWCNT following the procedure proposed by Reyes-Cruzaley *et al*. (2019).

2.1 Carbon nanocomposites

GO was prepared according to the procedure reported by Tour *et al*., (2010) with slight modifications proposed to improve the Hummers method (Hummers and Offeman 1958). Briefly, 3 g of graphite were oxidized using $NaNO_3$ and $KMnO_4$ in H_2SO_4 (conc.) The product was washed using water and H_2O_2. The purification process was modified, only HCl (5% v/v) was used to wash. Followed, the precipitate was washed with water until it reached a pH of 7. The final product was collected and dried in stove for 12 h at 60 °C.

We proposed a novel green method to synthesize nanocomposites of M/rGO (M = Co, Cu). 10 mg of GO were placed in a vial of 30 mL and dispersed in 10 mL of water at an ultrasound bath (BRANSON 3800, 40 kHz). For Co NPs, 0.308 mmol of $CoCl_2$ were dissolved in 10 mL of water and added to the before solution. Afterward, the metallic ions were reduced with 0.196 mmoles of $NaBH_4$, and the mixture was left to react for 60 min, maintaining the reaction temperature at 25 °C. For Cu NPs, 0.044 mmol $CuSO_4{\cdot}5H_2O$ were added, following the same procedure. The final product was filtered and washed with water and acetone. All reactions were carried at an ultrasound in this method. A similar procedure was reported by our research group to nanocomposites of M/MWCNT (Cu NPs) (Rivera-

Lugo *et al*., 2018). Subsequent, 2 mg of M/rGO was dispersed in an ultrasound bath in a mixture of 550 μL of ethanol and 150 μL of Nafion® for catalytic inks (Pollet 2014). The same procedure was done for each spacer. Next, M/rGO ink was kept at volume constant, adding the spacer ink in a proportion of 25, 50, 75 and 100 (% v/v). The final inks were sonicated to homogenize and labeled as Co/rGO/MWCNT, Co/rGO/CB, Cu/rGO/MWCNT, and Cu/rGO/CB.

2.2 *Physicochemical and electrochemical characterization*

The thermal behavior of nanocomposites was studied by thermogravimetric analysis (TA Instruments, TA-2960-DSC), heating at 20 °C·min^{-1} in airflow of 40 mL·min^{-1}. The identification of the crystalline phases was analyzed using a diffractometer (D8 Advance, Bruker) in Bragg-Brentano configuration. The intensity data were collected with 2θ ranging from 20 to 80° with 0.018 of step-size and 190 s of step-time. The morphology of NPs was determined by field-emission scanning electron microscopy (FE-SEM JEOL, JSM-7500F) and complemented using a high-resolution transmission electron microscopy (TEM JEOL JEM 2200FS+CS). A potentiostat/galvanostat (Biologic, VMP-300) was used for all the electrochemical tests. A three-electrode cell was occupied at room temperature (25 ± 1 °C) with 0.1 M of NaOH as the electrolytic solution. The working electrode (WE) was a glassy carbon rotating disk electrode (RDE, area: 0.2 cm^2), the reference electrode was Hg/HgO/NaOH$_{(1M)}$ and the counter electrode a Pt wire. The WE surface was modified using catalytic inks, keeping the ratio of 0.11 mg M/rGO. Cyclic voltammograms (CV) were performed in the potential range from -0.6 to 0.6 V vs. Hg/HgO/NaOH$_{(1M)}$ at a scan rate of 50 mV·s^{-1} (not shown). Catalytic activity for ORR was evaluated by linear sweep voltammetry at 0, 100, 250, 500, 750, 1000 and 1600 rpm controlled by Pine Instrument model AFMSRCE rotator, where the electrolyte was saturated with O_2. The electrochemical evaluation was done in the potential range from 0.5 to -1.2 V at a scan rate of 10 mV·s^{-1}. All potentials were reported vs. the standard hydrogen electrode (SHE). Finally, we carried out the accelerated durability tests (ADT), the procedure comprised continuous CV with ORR measurements at 0 and 3000 cycles (under the same conditions as described above).

3 Results and discussion

3.1 *Physicochemical characterization*

Fig. 1a shows the thermograms of carbonaceous species. For GO, the analysis of the curves of weight loss (%w) indicates three decomposition stages. The first stage comprises the range from 33 to 127 °C and corresponds to 2.0%; which is related to the desorption of moisture (Jeong *et al*., 2008; Ren *et al*., 2011). The second stage starts 156 °C and ends around 175 °C, which has the highest weight loss (96.2%) attributed to the decomposition of graphene layers containing labile oxygenated groups (Jeong *et al*., 2009). The third stage limits between 400 °C - 443 °C that has been related to the loss of stable oxygenated groups (Shen *et al*., 2009), presenting the lowest weight loss (1.2%). The final residue is 0.6% that attributed to potassium salts. For MWCNT, only one slope is observed between 525 °C and 700 °C. The metallic residue was 7.7%, which is associated with Fe_2O_3 of iron growth seed of MWCNT.

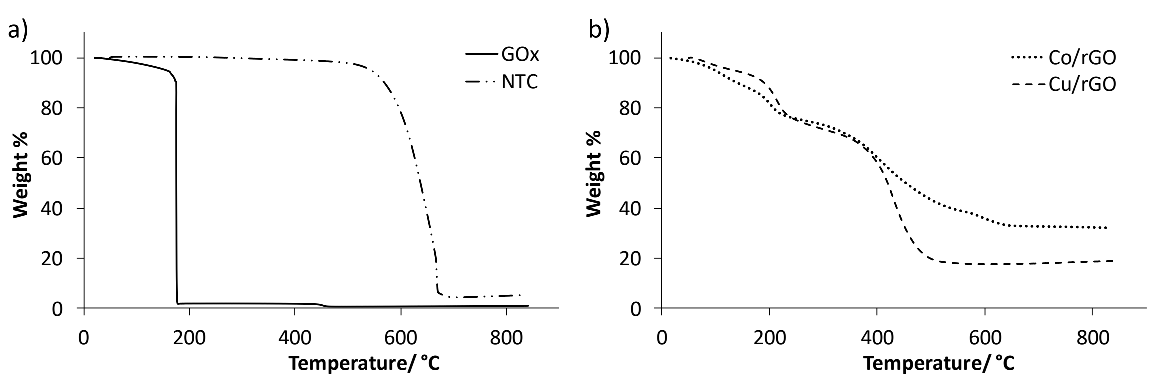

Fig. 1. Thermogravimetric curves of a) carbon nanotubes and graphene oxide; b) Co/rGO and Cu/rGO.

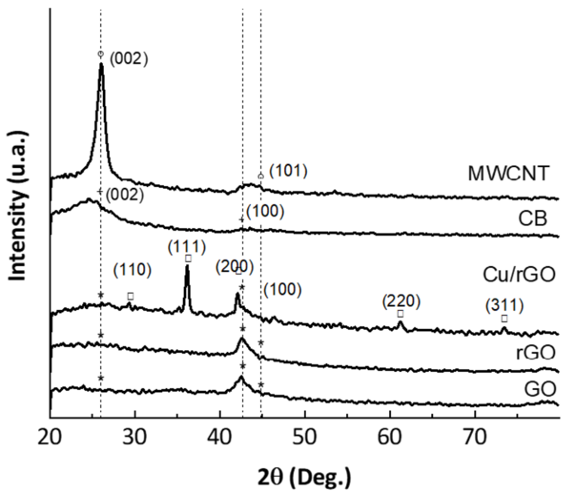

Fig. 2. XRD patterns of M/rGO nanocomposites and carbon spacers.

Fig. 1b shows the thermal behaviors of nanocomposites. Both materials presented the three weight losses, the first is related to the decomposition of graphene oxide at 200 °C (Jeong *et al*., 2009), following the second associated with the decomposition of rGO at 400 °C (Wilson *et al*., 2009), and the graphite decomposition at 600 °C. For Co/rGO, the metal deposition (i.e., the percentage of M^0 was calculated from the subtraction of MO_x) was 26.81%, while 14.60% for Cu/rGO.

Fig. 2 shows XRD patterns of supports, spacers and M/rGO nanocomposites. The graphene supports (GO and rGO) showed three diffracted intensity peaks at 24.66 (002), 42.57 (100) and 44.48° (101) that indexed to the graphite structure (JCPDS card No. 75-1621). Besides, the XRD patterns of used carbon spacers: MWCNT and CB indexed the identical graphite structure. The nanocomposite of Cu/rGO also showed five diffracted intensity peaks that can attribute to the structure of Cu_2O (JCPDS card No. 00-005-0667, space group Pn-3m (224) cubic, a = 0.426960 nm). In contrast, the intensity peaks of the cobalt phases were indiscernible; however, similar synthesized materials have been shown CoO (Rashad *et al*., 2020; Liang *et al*., 2020). The result suggests that the rGO surfaces were covered with nanoparticles of copper or cobalt oxide.

Fig. 3 shows the HRTEM image of Cu NPs and the FE-SEM image of Co NPs. Both nanoparticles were grown on the rGO sheets surface with a spherical shape. The Cu NPs covered all surfaces showing a small number of agglomerations (Fig. 3a); in contrast, the Co NPs were well-defined and isolated (Fig 3b). The average particle diameter (d_p) was 2.5±0.3 nm for Cu NPs and 7.2±1.4 nm for Co NPs. Fig. 3c shows the Gaussian probability density curves for d_p ($p > 0.05$) there is clear that the distribution of Cu NPs is denser than Co NPs. Likewise, the crystallite size (D_v) was calculated by the Scherrer's formula: $D_v = K\lambda/\beta\cos\theta$. Where $K = 0.94$ is a dimensionless shape factor, $\lambda = 1.54$ nm is the X-ray wavelength, β is the line broadening at half the maximum intensity (FWHM) and θ is the Bragg angle. The crystallite size was 2.2 nm, using the diffracted intensity peak at 36.2 (111) for Cu/rGO.

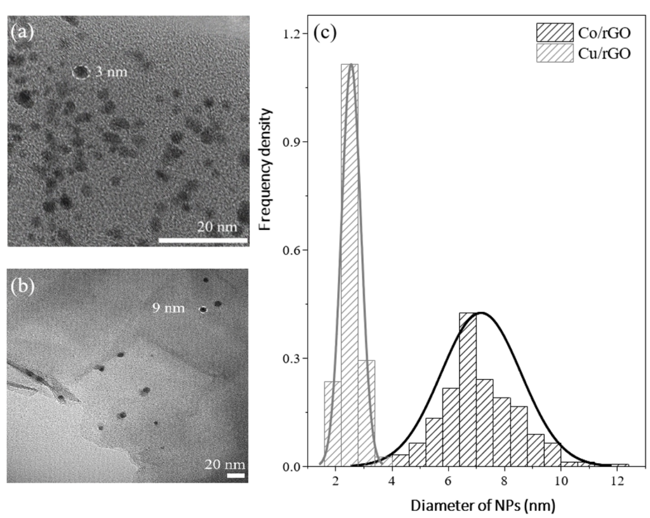

Fig. 3. Particle analysis: (a) Cu NPs, (b) Co NPs, and (c) density histograms of particle diameter for Co and Cu NPs.

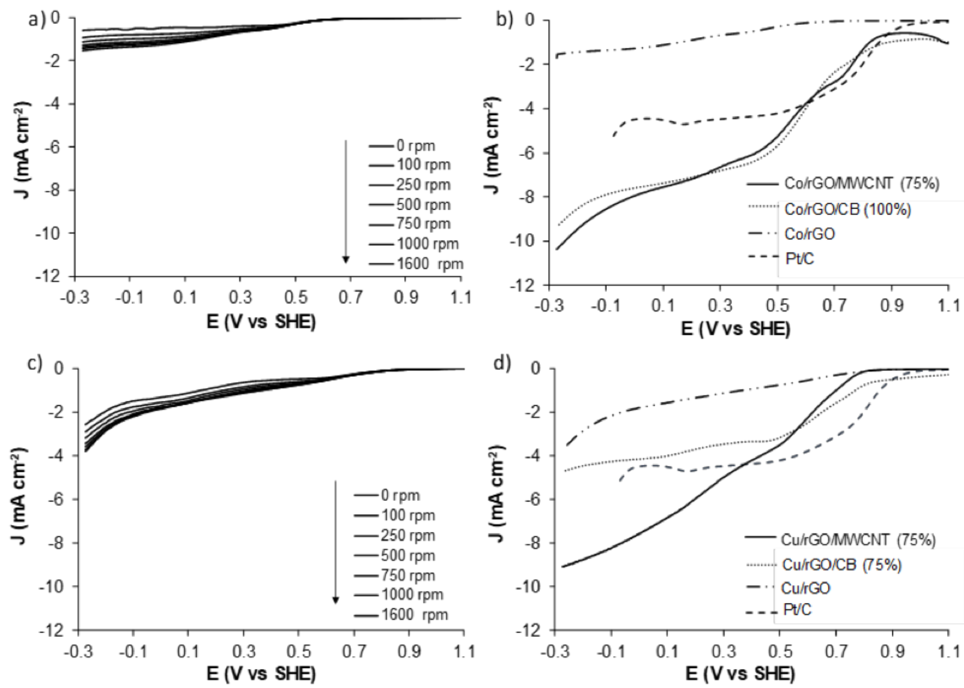

Fig. 4. Polarization curves of a) Co/rGO, b) Co/rGO with spacers, c) Cu/rGO and d) Cu/rGO with spacers at 1600 rpm.

3.2 *Electrochemical characterization*

We analyzed ORR for all treatment (M/rGO/MWCNT and M/rGO/CB) and levels (0, 25, 50, 75, and 100%). From data, the highest current densities (mA·cm^{-2}) were -9.43 (Co/rGO/MWCNT, 75%), -7.91 (Co/rGO/CB, 100%), -8.48 (Cu/rGO/MWCNT, 75%), -4.23 (Cu/rGO/CB, 75%), also the free spacers catalysts -1.36 (Co/rGO) and -2.39 (Cu/rGO) and the commercial platinum catalyst -5.23 (Pt/C). All evaluated nanomaterials were referenced at -0.1 V vs. SHE. Fig. 4 shows the polarization curves, comparing catalysts of carbon nanocomposites and free spacers. The number of electrons transferred (n) was four for all evaluated nanomaterials, which was determined through Koutecký-Levich (K-L) equation (Bard and Faulkner 2001).

Moreover, the Faradic charge resistance (R_{CT}) was calculated from the Butler-Volmer equation at $|F\eta| \ll RT$ (Rivera-Lugo *et al*. 2018). The R_{CT} values (Ω·cm^2) of the carbon nanocomposites were 0.46×10^{-3} (Co/rGO/MWCNT, 75%), 0.22×10^{-3} (Co/rGO/CB, 100%), 4.26×10^{-3} (Cu/rGO/MWCNT, 75%) and 0.78×10^{-3} (Cu/rGO/CB, 75%). Besides, the RCT values for free spacers catalysts were 209.28×10^{-3} (Co/rGO) and 53.61×10^{-3} (Cu/rGO). The spacers incorporation improved the conductivity of the cathode, where CB was outstanding up to 950 times for Co NPs and 68 times for Cu NPs. Fig. 5 shows a bar chart about the ADT comparison of the ORR performance evaluated at 0 and 3000 cycles. The spacers use provided higher stability in Cu NPs; only 12% of catalytic activity was a loss for MWCNT and unchanged for CB after 3000 cycles. In Co NPs, both spacers non-contribute to the stability of the catalytic activity.

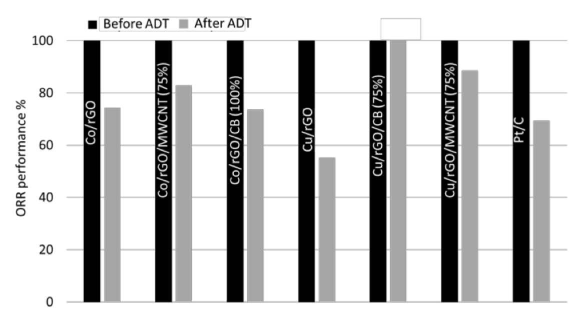

Fig. 5. Stability results of all evaluated nanomaterials.

The results indicate that the use of carbon spacers to separate graphene layers increments current density and decreases the Faradic charge resistance allowing the electrons flow in M/rGO/MWCNT

Table 1. Cobalt-graphene and copper-graphene systems previously reported in literature.

Ref.	Material	Particle size (nm)	Catalyst loading in WE (mg·cm^{-2})	Current density (mA·cm^{-2})
		Cobalt system		
Yang *et al*. (2018)	Co-N, S-G	~2.0	0.15	~-5.6
Niu *et al*. (2019)	Co@G/N-GCNs	17.0-18.0	0.25	~-5.7
Wang *et al*. (2017)	Co-N/G	20.0-50.0	0.24	~-5.1
This work	Co/rGO/MWCNT	7.0	0.55	-9.4
		Copper system		
Han *et al*. (2019)	Cu/G	Single atom	0.40	-5.6
Lv *et al*. (2014)	Pd-Cu NCs/rGOs	6.8	0.24	-4.6
Zheng *et al*. (2015)	G-Cu3Pd NCPs	5.3	—	-3.0
This work	Cu/rGO/MWCNT	2.2	0.55	-8.5

and M/rGO/CB. Likewise, the stability on the ORR performance increases in Cu/rGO/MWCNT and Cu/rGO/CB. These findings are consistent with that of Şanli *et al*. (2017) who show that CB into graphene layers reduces total resistance in the mass transport, improves the diffusion rate of oxygen to the catalytic sites and avoids graphene restacking, so incrementing their performance. Huang *et al*. (2012) indicate that CB increases the durability of the catalyst, agreeing with our results. About the use of MWCNT as a spacer, Cheng *et al*. (2013) reported the increasing mechanical stability and higher electrical conductivity, facilitating the electron transport, providing a large surface area and chemical stability, so the enhancing catalyst (Li *et al*. 2019). Another important finding was that the ORR performance of carbon nanocomposites was kept or improved comparing to free spacers catalysts or Pt/C.

In literature, there are a few reports about cobalt-graphene and copper-graphene systems (Table 1). For Co NPs, the size reported varied from 2 nm to 50 nm, showing current densities from -5.1 to 5.7 mA·cm^{-2}, as can be seen in Table 1. Our Co NPs presented a diameter of 7 nm, which lead us to infer that the improvement in the current densities reported compared to ours is the use of MWCNT spacer instead of particle size. In the case of copper system, we investigate that besides nanocomposites there is also graphene doping with Cu atoms, where an atom of copper substitutes an atom of carbon in graphene network (Yang *et al*., 2018), obtaining a current density of -5.6 mA·cm^{-2}. Also, we studied two reports of copper NPs, where the noble metal Pd was used, with particle size of 6.8 and 5.3 nm, and current densities of -4.6 and -3.0 mA·cm^{-2}, being lower than our ORR results. In this system, our Cu NPs are smaller than reported (less than twice of size), demonstrating that a Cu NP of 2 nm in diameter along with MWCNT spacer shows higher performance for ORR.

Conclusions

In summary, we prepared carbon nanocomposites using MWCNT and CB spacers from nanocomposites of Co and Cu NPs on rGO. The results showed that the use of spacers increases the current density, conductivity, and lifetime of the catalyst. The ORR performance can be equal to or better than that of Pt catalysts. The findings will be of interest for the generation of Pt free catalysts and more stable for ORR in alkaline media.

Acknowledgements

This work was financially supported by SENER-CONACyT of Mexico (292862). Yazmín Yorely Rivera Lugo wishes to thank CONACyT for the scholarship provided for her doctorate science research (scholar fellow 328834).

References

Akhina, H., Arif, P. M., Nair, M. R. G., Nandakumar, K., Thomas, S. (2019). Development of plasticized poly (vinyl chloride)/reduced graphene oxide nanocomposites for energy storage applications. *Polymer Testing 73*, 250-257.

Akhina, H., Nair, M. R. G., Kalarikkal, N., Pramoda, K. P., Ru, T. H., Kailas, L., Thomas, S. (2017). Plasticized PVC graphene nanocomposites: Morphology, mechanical, and dynamic mechanical properties. *Polymer Engineering Science 58*, E104-E113.

Arshad, A., Ali, H.M., Habib, A., Bashir, M.A., Jabbal, M. and Yan, Y. (2019). Energy and exergy analysis of fuel cells: A review. *Thermal Science and Engineering Progress 9*, 308-321.

Bard, A.J. and Faulkner, J.R. (2001). In: *Electrochemical Methods: Fundamental and Applications*, p. 341. John Wiley & Sons, New York.

Cheng, Y., Zhang, H., Varanasi, C.V. and Liu, J. (2013). Highly efficient oxygen reduction electrocatalysts based on winged carbon nanotubes. *Scientific Reports 3*, 3195-3199.

Ediger, V.Ş. (2019). An integrated review and analysis of multi-energy transition from fossil fuels to renewables. *Energy Procedia 156*, 2-6.

Flores, R., Muñoz-Ledo, R., Flores, B.B. and Cano, K.I. (2008). Power generation from biomass estimation for projects of the clean development mechanism program. *Revista Mexicana de Ingeniería Química 7*, 35-39.

Fu, K., Wang, Y., Mao, L., Jin, J., Yang, S. and Li, G. (2018). Facile morphology controllable synthesis of PtPd nanorods on graphene-multiwalled carbon nanotube hybrid support as efficient electrocatalysts for oxygen reduction reaction. *Materials Research Bulletin 108*, 187-194.

Garapati, M. S. and Sundara, R. (2019). Highly efficient and ORR active platinum-scandium alloy-partially exfoliated carbon nanotubes electrocatalyst for proton exchange membrane fuel cell. *International Journal of Hydrogen Energy 44*, 10951-10963.

Han, G., Zheng, Y., Zhang, X., Wang, Z., Gong, Y., Du, C., Banis, M. N., Yiu, Y-M., Sham, T-K., Gu, L., Sun, Y., Wang, Y., Wang, J., Gao, Y., Yin, G., Sun, X. (2019). High loading single-atom Cu dispersed on graphene for efficient oxygen reduction reaction. *Nano Energy 66*, 104088.

Hummers, W.S. and Offeman, R.E. (1958). Preparation of graphitic oxide. *Journal of the American Chemical Society 80*, 1339.

Jeong, H.K., Lee, Y.P., Lahaye, R.J.W. E., Park, M.H., An, K.H., Kim, I.J., Yang, C.W., Park, C.Y., Ruoff, R.S. and Lee, Y.H. (2008). Evidence of nearly flat layers and AB stacking order of graphite oxides. *Journal of the American Chemical Society 130*, 1362- 1366.

Jeong, H-K., Lee, Y.P., Jin, M.H., Kim, E.S., Bae, J.J. and Lee, Y.H. (2009). Thermal stability of graphite oxide. *Chemical Physics Letters 470*, 255-258.

Korkmaz, S., Kariper, I. A. (2020). Graphene and graphene oxide based aerogels: Synthesis, characteristics and supercapacitor applications. *Journal of Energy Storage 27*, 101038.

Li, K., Li, H., Li, M., Su, L., Qian, L. and Yang, B. (2019). Carbon-nanotube@graphene core-shell nanostructures as active material in flexible symmetrical supercapacitors. *Composites Science and Technology 175*, 92-99.

Li, Y., Li, Y., Zhu, E., McLouth, T, Chiu, C. Y., Huang, X. and Huang, Y. (2012). Stabilization of high-performance oxygen reduction reaction Pt electrocatalyst supported on reduced graphene oxide/carbon black composite. *Journal of the American Chemical Society 134*, 12326-12329.

Li, Y., Li, Z., Lei, L., Lan, T., Li, Y., Li, P., Lin, X., Liu, R., Huang, Z., Fen, X. and Ma, Y. (2019). Chemical vapor deposition-grown carbon nanotubes/graphene hybrids for electrochemical energy storage and conversion. *FlatChem 15*, 100091-100108.

Liang, B., Zhao, Y., Li, K., Lv, C. (2020). Porous carbon codoped with inherent nitrogen and externally embedded cobalt nanoparticles as a high-performance cathode catalyst for microbial fuel cells. *Applied Surface Science 505*, 144547.

Lv, J-J., Li, S-S., Wang, A-J., Mei, L-P., Feng, J-J., Chen, J-R., Chen, Z. (2014). One-pot synthesis of monodisperse palladium-copper nanocrystals supported on reduced graphene oxide nanosheets with improved catalytic activity and methanol tolerance for oxygen reduction reaction. *Journal of Power Sources 269*, 104-110.

Marcano, D.C., Kosynkin, D.V., Berlin, J.M., Sinitskii, A., Sun, Z., Slesarev, A., Alemany, L.B., Lu, W. and Tour, J.M. (2010). Improved synthesis of graphene oxide. *ACS Nano 4*, 4806-4814.

Marinkas, A., Arena, F., Mitzel, J., Prinz, G.M., Heinzel, A., Peinecke, V. and Natter, H. (2013). Graphene as catalyst support: the influences of carbon additives and catalyst preparation methods on the performance of PEM fuel cells. *Carbon 58*, 139-150.

Mukherjee, M., Samanta, M., Sarkar, S., Das, G. P., Chattopadhyay K. K. (2019). Graphene wrapped organic nanotube: A promising material for oxygen reduction reaction. *Materials Letters 248*, 8-11.

Niu, H-J., Zhang, L., Feng, J-J., Zhang, Q-L., Huang, H., Wang, A-J. (2019). Graphene-encapsulated cobalt nanoparticles embedded in porous nitrogen-doped graphitic carbon nanosheets as efficient electrocatalysts for oxygen reduction reaction. *Journal of Colloids Interfacial Science 552*, 744-751.

Norskov, J.K., Rossmeisl, J., Logadottir, A. and Lindqvist, L. (2004). Origin of the overpotential for oxygen reduction at a fuel-cell cathode. *Journal of Physical Chemistry B 108*, 17886-17892.

Ortiz-Salinas, R., Cram, S., Sommer, I. Polycyclic aromatic hydrocarbons (pahs) in soils of the low alluvial plain in the state of Tabasco, Mexico. *Revista Mexicana de Ingeniería Química 28*, 131-144.

Pan, Z.F., An, L., Zhao, T.S. and Tang, Z.K. (2018). Advances and challenges in alkaline anion exchange membrane fuel cells. *Progress in Energy and Combustion Science 66*, 141-175.

Park, S., Shao, Y., Wan, H., Rieke, P.C., Viswanathan V.V., Towne, S.A. and Wang, Y. (2011). Design of graphene sheets-supported Pt catalyst layer in PEM fuel cells. *Electrochemistry Communications 13*, 258-261.

Pollet, B.G. (2014). Let´s not ignore the ultrasonic effects on the preparation of fuel cell materials. *Electrocatalysis 5*, 330-343.

Rashad, M., Asif, M., Shah, J. H., Li, J., Ahmed, I. (2020). Simple synthesis of graphitic nanotube incorporated cobalt nanoparticles for potassium ion batteries. *Ceramics International 46*, 8862-8868.

Ren, P-G., Yan, D-X., Ji, X., Chen, T., Li, Z-M. (2011). Temperature dependence of graphene oxide reduced by hydrazine hydrate. *Nanotechnology 22*, 055705 (8pp).

Reyes-Cruzaley, A.P., Felix-Navarro, R.M., Trujillo-Navarrete, B., Silva-Carrillo, C., Zapata-Fernandez, J.R., Romo-Herrera, J.M., Contreras, O.E. and Reynoso-Soto, E.A. (2019). Synthesis of novel Pd NP-PTH-CNTs hybrid material as catalyst for H_2O_2 generation. *Electrochimica Acta 296*, 575-581.

Rivera-Lugo, Y.Y., Salazar-Gastélum, M.I., López-Rosas, D.M., Reynoso-Soto, E.A., Pérez-Sicairos, S., Velraj, S., Flores-Hernández, J.R. and Félix-Navarro, R.M. (2018). Effect of template, reaction time and platinum concentration in the synthesis of PtCu/CNT catalyst for PEMFC applications. *Energy 148*, 561-570.

Şanli, L.I., Bayram, V., Ghobadi, S., Düzen, N. and Gürsel, S.A. (2017). Engineered catalyst layer design with graphene-carbon black hybrid supports for enhanced platinum utilization in PEM fuel cell. *International Journal of Hydrogen Energy 42*, 1085-1092.

Shahid, M. M., Rameshkumar, P., Basirun, W. J., Ching, J. J., Huang, N. M. (2017). Cobalt oxide nanocubes interleaved reduced graphene oxide as an efficient electrocatalyst for oxygen reduction reaction in alkaline medium. *Electrochimica Acta 237*, 61-68.

Shen, J., Hu, Y., Shi, M., Lu, X., Qin, C., Li, C. and Ye, M. (2009). Fast and facile preparation of graphene oxide and reduced graphene oxide nanoplatelets. *Chemistry of Materials 21*, 3514-3520.

Song, A., Cao, L., Yang, W., Yang, W., Wang, L., Ma, Z., Shao, G. (2019). In situ construction of nitrogen-doped graphene with surface-grown carbon nanotubes as a multifactorial synergistic catalyst for oxygen reduction. *Carbon 142*, 40-50.

Valdez-Ojeda, R., Aguilar-Espinosa, M., Gómez-Roque, L., Canto-Canché, B., Escobedo Gracia-Medrano, R.M., Domínguez-Maldonado, J. and Alzate-Gaviria, L. (2014). Genetic identification of the bioanode and biocathode of a microbial electrolysis cell. *Revista Mexicana de Ingeniería Química 13*, 573-581.

Vanýsek, P. (2009). In: *CNC Handbook of Chemistry and Physics*, (Taylor and Francis Group), p. 23. CRC Press, Boca Raton.

Wang, Q., Hu, W., Huang, Y. (2017). Nitrogen doped graphene anchored cobalt oxides efficiently bi-functionally catalyze both oxygen reduction reaction and oxygen revolution reaction. *International Journal of Hydrogen Energy 42*, 5899-5907.

Wilson, N.R., Pandey, P.A., Beanland, R., Young, R.J., Kinloch, I.A., Gong, L., Liu, Z., Suenaga, K., Rourke, J.P., York, S.J. and Sloan, J. (2009). Graphene oxide: structural analysis and applications as a highly transparent support for electron microscopy. *ACS Nano 3*, 2547-2556.

Wu, D-Y., Zhou, W-H., He, L-Y., Tang, H-Y., Xu, X-H., Ouyang, Q-S., Shao, J-J. (2020). Micro-corrugated graphene sheet enabled high-performance all-solid-state film supercapacitor. *Carbon 160*, 156-163.

Yan, Z., Gao, L., Dai, C., Zhang, M., Lv, X. and Shen, P.K. (2018). Metal-free mesoporous carbon with higher contents of active N and S cooping by template method for superior ORR efficiency to Pt/C. *International Journal of Hydrogen Energy 43*, 3705-3715.

Yang, H. B., Guo, C., Zhang, L., Hu, F. X., Cai, W., Gao, J., Li, C. M., Liu, B. (2018). Nitrogen and sulfur Co-doped graphene inlaid with cobalt clusters for efficient oxygen reduction reaction. *Materials Today Energy 10*, 184-190.

Yilmaz, M. S., Kaplan, B. Y., Gürsel, S., Metin, Ö. (2019). Binary CuPt alloy nanoparticles assembled on reduced graphene oxide-carbon black hybrid as efficient and cost-effective electrocatalyst for PEMFC. *International Journal of Hydrogen Energy 44*, 14184-14192.

Yurtcan, A. B., Daş, E. (2018). Chemically synthesized reduced graphene oxide-carbon black based hybrid catalysts for PEM fuel cells. *International Journal of Hydrogen Energy 43*, 18691-18701.

Zheng, Y., Zhao, S., Liu, S., Yin, H., Chen, Y-Y., Bao, J., Han, M., Dai, Z. (2015). Component-controlled synthesis and assembly of Cu-Pd nanocrystals on graphene for oxygen reduction reaction. *ACS Applied Materials Interfaces 7*, 5341-5357.